

Short vs. Long-term Coordination of Drones: When Distributed Optimization Meets Deep Reinforcement Learning

Chuhao Qin*, and Evangelos Pournaras*

*School of Computing, University of Leeds, Leeds, UK

Abstract—Swarms of autonomous interactive drones can provide compelling sensing capabilities in Smart City applications, such as traffic monitoring. This paper focuses on the task assignment problem for large-scale spatio-temporal sensing by a drone swarm. However, existing approaches have distinct challenges: evolutionary distributed optimization, such as collective learning, lacks long-term adaptability in dynamic environments, while deep reinforcement learning (DRL) is limited to scale effectively due to the curse of dimensionality. Therefore, this paper proposes a novel synergetic optimization approach by integrating long-term DRL and short-term collective learning. Through this approach, each drone independently and proactively determines its flying direction and recharging location using DRL, while evolving their navigation and sensing policies through collective learning based on a structured tree communication model. Extensive experiments with datasets generated from realistic urban mobility demonstrate an outstanding performance of the proposed solution in complex scenarios. New insights show that this approach provides a win-win synthesis of short-term and long-term strategies for drone-based traffic monitoring, with short-term methods addressing training complexity and energy management, while long-term methods preserving high sensing performance.

Index Terms—drones, UAV, navigation, sensing, recharging, distributed optimization, deep reinforcement learning

I. INTRODUCTION

Unmanned Aerial Vehicles (UAVs), referred to as drones, can organize themselves into swarms, fostering collaboration and efficiency in sensor data collection within Smart Cities [1]. With their mobility, autonomy, and diverse sensors, drones have been widely used in several applications, such as monitoring traffic congestion [2] and mapping natural disasters [3]. Despite these advantages, drones are constrained by limited battery capacity, which impacts their spatio-temporal coverage. This limitation necessitates sophisticated autonomous control systems and precise task assignment within drone swarms. This involves the assignment of different sensing tasks to each drone while meeting the sensing requirements, drone capabilities and constraints [4]. Recently, scholars have solved the NP-hard combinatorial optimization problem of task assignment for spatio-temporal sensing, using evolutionary algorithms ranging from genetic algorithms to swarm intelligence methods [4], [5]. To enhance robustness and minimize the effects of individual drone failures, distributed optimization approaches have been introduced. These approaches allow

drones to autonomously self-organize and self-assign tasks in a decentralized manner, preserving the autonomy of individual drones. However, these distributed approaches are reactive to the current state of the environment rather than proactive to address long-term operational challenges strategically.

Strategic foresight in navigation and sensing is crucial for optimizing drone operations in dynamic environments, significantly influenced by flying directions and future sensor data requirements. For example, drones aware of an expected increase in traffic can proactively fly to those areas, improving tasks such as vehicle detection, even if the short-term benefits are not evident. This "slower is faster" effect emphasizes the importance of long-term planning for overall effectiveness in drone sensing. To address long-term optimization, deep reinforcement learning (DRL) has been introduced, utilizing the Bellman equation to consider cumulative rewards [6]. DRL based on deep neural networks support drones, as heterogeneous agents, to manage complex state spaces and adapt to changing environments.

However, traditional DRL approaches cannot scale well with a large number of agents and extended time spans due to the curse of dimensionality. With more agents, coordinating them becomes exponentially more complex, leading to computational challenges. Furthermore, DRL methods need to account of environmental uncertainties and the long-term consequences of agents' actions, which become increasingly complex as the time horizon extends. For example, drones often make flight path decisions over short intervals, such as seconds or minutes, but face significant challenges when required to adapt their policies for a long duration (e.g., a full day). Meanwhile, the extended operation is longer than the maximum flight time of drones, enabling them to return to a base station for recharging and depart from that place for the subsequent task. The selection of these recharging places constraints the drones' flight ranges, which in turn affects their sensing performance.

Therefore, in this paper, we address a novel task assignment problem for large-scale spatio-temporal sensing, focusing on the navigation (determining flight path), sensing (scheduling data collection) and recharging (choosing charging stations as destinations) of drone swarms in changing environments. To jointly manage these tasks, we propose a new synergetic optimization approach to coordinate drone swarms through Distributed Optimization and (deep) Reinforcement Learning (*DO-RL*), which involves a multi-agent DRL algorithm that builds upon on an iterative collective learning approach [7],

[8]. It allows drones to determine long-term flying directions from departures to destinations (i.e., charging stations) via DRL, while autonomously evolving their short-term navigation and sensing policies based on shared plans from other drones through collective learning. The distributed sensing results generated during operations serve as rewards and observations for further DRL training. These results are aggregated and shared using a structured tree communication model, where each drone interacts with its parent and child nodes, making independent decisions. This ensures scalability (supporting a large number of agents), efficiency (low communication and computational cost), decentralization and resilience [9]–[11]. By employing this collaborative approach, collective learning reduces the frequency of decision-making and mitigates inefficient actions, effectively compensating for the limitations of DRL while retaining its strengths in long-term planning and optimization. In addition, a set of auxiliary approaches is introduced, including plan generation, plan selection, periodic state updates and a centralized training and decentralized execution module. To validate *DO-RL*, this paper conducts experimental evaluations with real-world data and emulated traffic monitoring scenarios, comparing it against state-of-the-art baseline methods.

The contributions of this paper are outlined as follows: (i) The first study of task assignment for large-scale, dynamic spatio-temporal sensing by a swarm of drones, concentrating on optimizing the flight paths, data collection strategies, and recharging. (ii) A novel synergetic optimization approach, *DO-RL*, that tackles this problem by integrating both multi-agent DRL and distributed optimization based on a structured tree communication model. (iii) A testbed for extensive experimentation with realistic traffic patterns and real-world transport networks. (iv) The validation for the superior performance of the proposed approach over three state-of-the-art methods. (v) An open-source implementation of the proposed approach and an open dataset [12] containing all plans of the studied scenario. They can be used as benchmarks to encourage further research on this problem.

TABLE I
COMPARISON TO RELATED WORK: CRITERIA COVERED (✓) OR NOT (✗).

Criteria	Ref.:	[13]	[14]	[15]	[16]	[17]	[18]	[19]	This paper
Decentralization		✓	✓	✓	✗	✗	✓	✗	✓
Long-term efficiency		✗	✗	✗	✓	✓	✓	✓	✓
Scalability		✗	✗	✓	✗	✗	✓	✗	✓
Resilience		✗	✗	✓	✗	✗	✗	✗	✓
Adaptability		✓	✓	✓	✓	✓	✗	✓	✓

II. RELATED WORK

Sensing task assignment. The UAV task assignment problem for spatio-temporal sensing has been traditionally defined as the Traveling Salesmen Problem [1], [20]. This involves finding the optimal assignment of tasks to drones at specific locations, while considering constraints such as task urgency, time scheduling, and flying costs. The evolutionary optimization methods, such as particle swarm optimization [21], and genetic algorithm [22], have been introduced to formulate the problem

of reaching optimal sensing efficiency in terms of coverage, events detection rate and the cost of flight paths. They rely on adaptive exploration of the solution space to optimize task allocation based on shared information and local interactions. However, these methods are centralized, wherein the failure of a central control station can lead to several system disruptions without autonomous recovery mechanisms [23].

Distributed optimization. Several distributed task assignment algorithms have been proposed. One such algorithm is the robust decentralized task assignment (RDTA) [13] that enhances robustness and reduces communication costs by employing decentralized planning for drones. Another one is the consensus-based bundle algorithm (CBBA) [14], which combines market-based mechanisms and situation awareness to converge and avoid task conflicts among drones. Moreover, a planning-based coordination method using collective learning, named Economic Planning and Optimized Selections (EPOS), enables drones to optimize their navigation and sensing options under battery constraints [15], [24]. However, long-term sensing scenarios pose challenges. Drones tend to prioritize immediate maximum returns in the short term, often neglecting the need for strategic decision-making for overall benefits.

DRL-based drone sensing. The deep reinforcement learning (DRL) algorithm proves to be effective for addressing distributed sensing with drones, managing complex optimization goals, energy constraints, and numerous heterogeneous agents. Ding *et al.* [16] integrated mobile crowdsensing (i.e., human equipped with mobile sensing devices) into UAV sensing, overcoming the limitations of both human mobility and drone battery life. Omoniwa *et al.* [25] presented a decentralized DRL approach that improves drone energy efficiency in providing wireless connectivity by sharing information with neighbouring drones. Zhao *et al.* [17] proposed a comprehensive solution for sustainable urban-scale sensing in open parking spaces. Their solution incorporates the task selection and scheduling using DRL, and adaptive recharging assignment. However, these approaches lack autonomy for drones in self-assignment tasks, reducing adaptability to the real-time environmental changes and increasing vulnerability to agent failures [23]. Additionally, they are confined to a small-scale task assignment problem due to the training complexity.

Evolutionary algorithm and DRL. In this optimization process, the related synergetic optimization algorithms integrate the full learning and optimization capabilities of evolutionary algorithms and DRL. They independently solve sub-problems to generate partial solutions, which are then combined to form a complete solution [26]. Earlier work [27], [28] has proposed optimizing team policies using evolutionary algorithms with team rewards, while simultaneously optimizing individual policies through DRL with agent rewards, thus bypassing the non-stationary problem in multi-agent DRL. Li *et al.* [18] introduce a hybrid framework using shared observation encoders and independent linear policy representations to enhance collaboration on complex task, ensuring stable evolution through agent-level crossover and mutation. While benchmarks, such as MuJoCo [29] and Starcraft II [30], are useful for evaluation of these approaches, these benchmarks

may struggle to adapt to the continuously evolving and unanticipated dynamics typical of real-world scenarios, such as fluctuating traffic patterns in drone-based monitoring systems.

Transportation application. In the application of transportation system, drones rely on accurate vehicle observation to detect early signs of traffic congestion. This enables traffic operators to apply mitigation measures, reducing the carbon footprint in one of the world's highest-emission sectors. El-loumi *et al.* [31] proposed a road traffic monitoring system that generates adaptive drones trajectories by extracting information about vehicles. Samir *et al.* [19] leveraged a DRL algorithm to optimize the trajectories of UAVs, with the objective of minimizing the age of information of collected data. While these approaches demonstrate high performance in the detection of traffic vehicles, scalability becomes a challenge since they only deal with a small number of drones within a short duration.

In summary, previous approaches have either neglected the long-term advantages of strategic sensing, or failed to effectively adapt to failures and scale without encountering centralized bottlenecks. To overcome these shortcomings, the proposed approach empowers drones to make informed and proactive decisions based on predicted traffic flow, while enabling them to independently adjust to changing conditions and unexpected events, ensuring both scalability and resilience without relying on centralized control.

III. SYSTEM MODEL

In this section, we define key concepts of scenarios and then formulate the main performance metrics.

A. Scenario and Assumptions

Sensing map. Consider a swarm of drones $\mathcal{U} \triangleq \{1, 2, \dots, U\}$ performing map sensing missions, such as monitoring vehicles, over a grid that represents a 2D map. In this scenario, a set of grid cells (or points of interest) $\mathcal{N} \triangleq \{1, 2, \dots, N\}$ are uniformly arranged to cover the map. The primary goal of the drones is to coordinate their visits to these cells to collect the required data. Furthermore, a set of charging stations $\mathcal{M} \triangleq \{1, 2, \dots, M\}$, from which the drones depart from and return to, are located at fixed coordinates on the map.

Time periods and slots. We assume a set of time periods as $\mathcal{T} \triangleq \{1, 2, \dots, T\}$. Each time period can be divided into a set of equal-length scheduling timeslots $\mathcal{S} \triangleq \{1, 2, \dots, S\}$. In each timeslot, a drone can be controlled to fly to a cell and hover to collect sensor data.

Action. To explain the long-term navigation and sensing over all periods, we introduce the period-by-period actions of each drone $a^u = \{0, 1, 2, \dots, 8\}$, $u \in \mathcal{U}$, meaning to control u to move horizontally along eight directions, which are 1 = north (N), 2 = east (E), 3 = south (S), 4 = west (W), 5 = northeast (NE), 6 = southeast (SE), 7 = southwest (SW), and 8 = northwest (NW), or return to the origin ($a^u = 0$). Under each action, u executes a short-term navigation and sensing. After completing its sensing tasks, u flies back to one of the charging stations to recharge fully and resume work in the next period $t + 1$.

Matrix of plans. To explain the short-term navigation and sensing of drones over the cells and timeslots in a period t , $t \in \mathcal{T}$, the plan of a drone u that travels through the direction of a^u is introduced, denoted by $P^u(a^u, t)$. It represents the specific navigation and sensing details, including the visited cells and corresponding energy consumption. The plan $P^u(a^u, t)$ is encoded by a matrix of size $N \times S$, with each element represented as $p_{n,s}^u(a^u, t) \in \{0, 1\}$. Here, $p_{n,s}^u(a^u, t) = 1$ denotes that the drone u hovers and collects all required data at cell n at timeslot s , whereas for $p_{n,s}^u(a^u, t) = 0$ the drone does not hover at that cell at that time. Moreover, $P^{-u}(a^u, t) = \{p_{n,s}^{-u}(a^u, t) | n \in \mathcal{N}, s \in \mathcal{S}\}$ denotes the observed plan by drone u in time period t , indicating that it incorporates and sums the plans of all other drones excluding its own. We formulate the aggregated plans of all drones observed by u at cell n and timeslot s as follows:

$$p_{n,s}(a^u, t) = p_{n,s}^u(a^u, t) + p_{n,s}^{-u}(a^u, t). \quad (1)$$

Matrix of required sensing values. In the context of a sensing task, each cell at a timeslot has specific sensing requirements that determine the data acquisition goal of drones. Such sensing requirements can be determined by city authorities as a continuous kernel density estimation, for example, monitoring cycling risk based on requirements calculated by past bike accident data and other information [15], [32]. The high risk level of a cell at a timeslot represents the high importance of sensing (e.g., the crucial intersection of traffic flow), and thus a high number of required sensing values is set. The matrix of required sensing values is denoted as $V(t) = \{V_{n,s}(t) | n \in \mathcal{N}, s \in \mathcal{S}\}$, where $V_{n,s}(t)$ denotes the required sensing value at cell n and timeslot s in the time period t . Based on actual sensing performance of drones according to Eq.(1), the sensing value collected by all drones observed by u at cell n and timeslot s is formulated as:

$$v_{n,s}(a^u, t) = p_{n,s}(a^u, t) \cdot V_{n,s}(t). \quad (2)$$

Matrix of target. In a real-world scenario, drones lack prior knowledge of the amount of required sensing values before they begin their sensing operations. Therefore, it becomes essential to build a target on the fly that instructs the drones regarding when and where they should or should not fly to given information from the environment. The matrix of the target is defined as $\mathcal{R}(t)$, which denotes the sensing requirements for all drones at period t . The element of the target is denoted as $r_{n,s}(t) = \{0, 1\}$, $n \in \mathcal{N}$, $s \in \mathcal{S}$, where $r_{n,s}(t) = 1$ requires only a drone to visit the cell n at timeslot s , and $r_{n,s}(t) = 0$ does not require sensor data collection by a drone.

Assumptions. To simplify the scenario, this paper makes the following assumptions: (i) Each drone is programmed to fly at a distinct altitude during its movement between cells to prevent mid-air collisions risks [33]. While previous work [34], [35] has explored a safe and cost-effective approach to a more realistic collision avoidance, this is not the primary focus of this paper. (ii) Each time period concludes a flying period and a charging period: the time that drones perform sensing, and the time for charging. All drones finish charging before

the next time period begins. We assume that each charging period is of equal duration and provides sufficient time for the drones to be fully charged. (iii) Each charging station is adequately equipped with charging capacity, enabling multiple drones to charge simultaneously without the need for queuing. This arrangement prevents any delays in the charging process.

B. Problem Formulation

We model the scenario of a swarm of drones that perform sensing by considering the following performance metrics: 1) mission efficiency; 2) sensing accuracy; and 3) energy cost.

Mission efficiency. It denotes the ratio of sensing values in all cells at all timeslots collected by the drones during their mission over the total required values in all cells at all timeslots during the period t . The purpose is to collect sensing data as much as possible. It is formulated as:

$$\text{Eff}(a^u, t) = \frac{\sum_{n=1}^N \sum_{s=1}^S v_{n,s}(a^u, t)}{\sum_{n=1}^N \sum_{s=1}^S V_{n,s}(t)}. \quad (3)$$

However, maximizing this metric leads to sensing imbalance and even blind areas. Some cells may be covered for a long time while some other cells may be never covered, i.e., the over-sensing and under-sensing [24]. Thus, it is necessary to consider matching indicators such as the sensing accuracy [24] to access such imbalances.

Sensing accuracy. It denotes the matching (correlation¹) between the total sensing values collected and the required ones. The metric is formulated as follows:

$$\text{Acc}(a^u, t) = \sqrt{\frac{N \cdot S}{\sum_{n=1}^N \sum_{s=1}^S [v_{n,s}(a^u, t) - V_{n,s}(t)]^2}}. \quad (4)$$

Apart from improving the efficiency and accuracy of drone sensing, the energy consumed by drones needs to be saved.

Energy cost. It is the battery usage of drones to perform spatio-temporal sensing. A power consumption model [36] is used to calculate the power consumption with input the specification of drones (weight, propeller and power efficiency). This model estimates the cost of navigation and sensing plans, and emulates the outdoor environments [15]. The energy cost of each drone u is formulated as:

$$E(a^u, t) = \frac{C^f(u) \cdot t^f(a^u) + C^h(u) \cdot t^h(a^u)}{B(u)}, \quad (5)$$

where $B(u)$ is the battery capacity of drone u ; $C^f(u)$ and $C^h(u)$ denote the flying and hovering power consumption of u respectively; t^f and t^h are the flying and hovering time respectively, which are determined by the sensing plan $P^u(a^u, t)$.

As described before, the optimization problem has three objectives: 1) maximize mission efficiency; 2) maximize sensing accuracy; and 3) minimize energy cost. Simultaneously achieving all of these objectives is a daunting task, as they often oppose each other. Maximizing both efficiency and

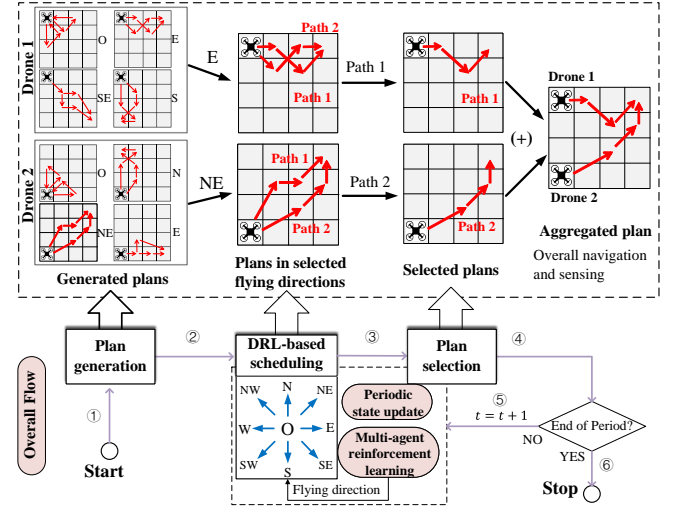


Fig. 1. System framework of *DO-RL*. The overall flow of *DO-RL* is depicted at the bottom; The plan selection is illustrated for two drones; The plan generation part outlines the procedure for generating a plan when drone 1 is traveling to the east.

accuracy is a trade-off. In addition, in order to achieve both of these goals, drones have to continuously move to collect data from different cells, which results in higher energy costs due to long-distance flights. However, some trips of drones may not improve sensing quality in the long run. For instance, at the end of a period, drones opt to return to the nearest charging station where there are fewer sensing tasks in the next period. This choice reduces the energy cost of the current period but comes at the significant expense of sacrificing the sensing quality in the next period. Therefore, the overall sensing performance is optimized by integrating these opposing objectives and selecting the plans of each drone.

Overall performance. The objective function is defined as the weighted sum of mission efficiency, sensing accuracy and energy cost:

$$\arg \max_{a^u, u \in \mathcal{U}} \sum_{u=1}^U \sum_{t=1}^T [\alpha_1 \text{Eff}(a^u, t) + \alpha_2 \text{Acc}(a^u, t) - \alpha_3 E(a^u, t)]. \quad (6)$$

IV. THE PROPOSED SOLUTION

A. System Overview

In our problem, traditional DRL approaches suffer from the large action space and dimensional curse caused by the increasing number of time periods, leading to decline in sensing quality. To ensure high-quality sensing performance, the proposed *DO-RL* integrates decentralized drone coordination for short-term navigation and sensing optimization with long-term scheduling of flying directions. Fig.1 illustrates the designed system framework of *DO-RL*, consisting of three main components:

Plan generation. This component generates the navigation and sensing options for drones. Given the sensing map, each drone autonomously generates a finite number of discrete plans

¹Error and correlation metrics (e.g. root mean squared error, cross-correlation or residuals of summed squares) estimate the matching, shown to be NP-hard combinatorial optimization problem in this context [7], [8].

B. Plan Generation

The actions enable each drone to generate nine groups of plans, each associated with an action for a flying direction. These groups consist of multiple individual plans of the same size. A group of plans generated by drone u during a period is defined as $G^{a^u}(t)$, where each plan in the group has the same action, $P^u(a^u, t) \in G^{a^u}(t)$. Then, a plan can be defined as $P^u(a^u, t) = \{l, K(a^u), J(a^u), E(a^u, t)\}$, where l is the index of the plan, $l \leq L$, (L denotes the total number of plans in a group); $K(a^u)$ denotes the indexes of cells within the searching range along flying direction a^u ; $J(a^u)$ denotes the indexes of visited cells within $K(a^u)$; and $E(a^u, t)$ denotes the energy consumed by u traveling over $J(a^u)$, i.e., the cost of the plan.

The details of generating a single plan are defined by the chosen path and the corresponding energy required to traverse that path, as shown in Fig. 3. As an example of a plan, the drone u firstly finds a searching range to cells $K(a^u)$: it determines a range with a certain width (equal to half of distance to nearest charging station) along its flying direction, and then searches the cells within this range. Next, it selects the visited cells $J(a^u)$ randomly from this range. Then, u finds the shortest possible path among $J(a^u)$ via the *Dijkstra's algorithm* for the Traveling Salesmen Problem. The path includes the information of which cell and which timeslot the drone uses to collect data, and thus both the traveling time $t^f(a^u)$ and sensing time $t^h(a^u)$ are calculated. The total energy consumption $E(a^u, t)$ when u travels over the path is then calculated via Eq.(5).

C. Plan Selection

Given the plans in selected flying directions within a period, drones can adapt their assignments by selecting appropriate plans in response to changes in task targets, enhancing their adaptability in dynamic environments. In this process, the agents of drones improve their plan selections via tree communication. Specifically, each agent obtains the aggregated choices, i.e., the aggregated plan $P^{-u}(a^u, t)$, from other agents, and chooses one of the plans $P^u(a^u, t, l)$ such that all choices together $P^u(a^u, t) + P^{-u}(a^u, t)$ add up to match a target $\mathcal{R}(t)$. The target is used to steer each drone to sense over a unique cell during a timeslot, thereby avoiding the simultaneous sensing of multiple drones within the same cell, i.e., preventing over-sensing and under-sensing.

The purpose of coordination is to match the aggregated plans of all agents to the target while minimizing the energy cost $E(a^u, t)$ of the plan selected by the drone. The cost function for each agent is formulated using the root mean square error (RMSE):

$$\min_{a^u, u \in \mathcal{U}} (1 - \beta) \cdot \sqrt{\frac{\sum_{n=1}^N \sum_{s=1}^S [p_{n,s}(a^u, t) - r_{n,s}(t)]^2}{N \cdot S}} + \beta \cdot E(a^u, t), \quad (7)$$

where β represents the behavior of an agent. As the value of β increases, the agent becomes increasingly selfish, prioritizing plans with lower energy costs at the expense of higher root

mean squared error. Each agent (or drone) aims to minimize the system-wide cost of sensing while considering its energy consumption. By minimizing this cost function, each drone coordinates to select its optimal plan, indicating a specific path within a period (comprising multiple timeslots). Via planning and selection, drones using *DO-RL* only need to take high-level actions of flying directions in each period, and thus reducing the number of decisions and observations in DRL.

D. Periodic State Update

After choosing a plan, each drone changes its current state at the next period $t + 1$, including its location $c^u(t + 1)$, battery level $e^u(t + 1)$, selected plan $P^u(t + 1) := P^u(a^u, t)$, and observed plan $P^{-u}(t + 1) := P^{-u}(a^u, t)$. However, due to dynamic changing environment, drones have no knowledge about the required sensing value in the next period. They need to predict and estimate the required sensing value to calculate reward function via Eq.(3) and (4). Depending on the predicted distribution of sensor data, the target is required to be updated.

Predicted sensing value. The predicted sensing value at period t , denoted as $\hat{V}(t)$, is updated in a time-reverse decay, formulated as follows:

$$\hat{V}_{n,s}(t) = \sum_{t'=1}^t (T-t+t') \cdot \omega_{n,s}(t') \cdot v'_{n,s}(a^u, t') := V_{n,s}(t), \quad (8)$$

where $V'_{n,s}$ denotes the data values collected by drones once they execute their selected plans; $\omega_{n,s}(t')$ is a prediction coefficient such that $0 < \omega_{n,s}(t') < 1$, $t' \leq t$. To achieve accurate predictions, *DO-RL* leverages the Ordinary Least Squares regression method (OLS) to train these coefficients initially, and use the past experienced observations as the target distribution for training.

Target. The target \mathcal{R} in the plan selection needs to be iteratively updated to steer the coordination of drones to choose plans for areas and timeslots with abundant sensor data. The percentile-based data filtering is used to eliminate the extreme low sensing values collected by drones. This approach effectively removes the need for data collection in regions with low sensing requirements (e.g., traffic exclusion zones). As a consequence, it helps drones in prioritizing their operations in cells and time where sensing values are significantly high. We initialize the target as $r_{n,s}(0) = 1$ to encompass all cells and timeslots, and update it as follows:

$$r_{n,s}(t) = \begin{cases} 0, & v'_{n,s}(a^u, t) < \bar{v} \wedge p_{n,s}(a^u, t) > 0 \\ r_{n,s}(t-1), & \text{otherwise} \end{cases}, \quad (9)$$

where the threshold \bar{v} is set iteratively and calculated as the value at the $100(1 - U/N)$ th percentile among the predicted data values $\hat{V}_{n,s}(t)$.

At the end of state update in *DO-RL*, the current collected data values $V'_{n,s}$, the predicted values $\hat{V}_{n,s}$ and the target \mathcal{R} are shared with each agent via the top-down interactions within the tree communication structure. This information will be stored and later sampled for multi-agent reinforcement learning.

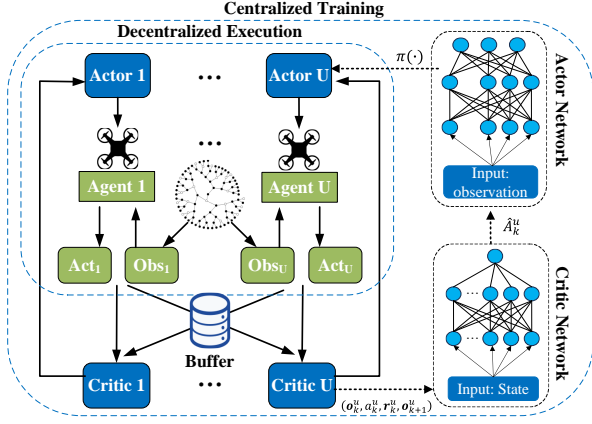


Fig. 4. DRL-based long-term scheduling overview.

E. Multi-agent Reinforcement Learning

Our approach provides a generalized model for multi-agent reinforcement learning by adopting the framework of centralized training and decentralized execution, as shown in Fig.4. During execution, each agent obtains a local aggregated observation comprising both private and public information. Apart from their own private data such as locations, battery levels, and selected plans, this observation contains aggregated plans shared via the tree communication model (shown in Fig. 2). The training part is built based on an actor-critic model. The actors allow drones to work independently and choose actions based on their observations and policies, allowing for parallel data collection and processing. The critic, however, evaluates the actions of drones and guide them toward collectively optimal decisions. In addition, *DO-RL* employs Proximal Policy Optimization (PPO) to prevent detrimental updates and improving the stability of the learning process [37].

The process of training primarily involves the following steps: Firstly, each agent takes an action for a flying direction based on the aggregated observation \mathbf{o}_t^u shared via coordination as well as the reward \mathbf{r}_t^u . Once all actions are determined, drones select their plans and transition to a new state. Subsequently, the buffer, a data storage structure used for experience replay, stores all transitions of each agent ($\mathbf{o}_t^u, \mathbf{a}_t^u, \mathbf{r}_t^u, \mathbf{o}_{t+1}^u$). Several groups of transitions ($\mathbf{o}_k^u, \mathbf{a}_k^u, \mathbf{r}_k^u, \mathbf{o}_{k+1}^u$) are sampled randomly (H groups of transitions) for updating the parameters of both the critic and actor networks. The algorithm is typically an extension of the actor-critic policy gradient approach, employing two deep neural networks for each agent: a critic network $Q(\cdot)$ and an actor network $\pi(\cdot)$. The critic network estimates the reward associated with a transition using Bellman equation, and its parameter θ^Q is then updated by minimizing a loss function $L(\theta^Q)$:

$$L(\theta^Q) = \frac{1}{H \cdot U} \sum_{k=1}^H \sum_{u=1}^U (\hat{A}_k^u)^2, \quad (10)$$

$$\hat{A}_k^u = \mathbf{r}_k^u + \gamma \cdot Q(\mathbf{o}_{k+1}^u, \mathbf{a}_{k+1}^u) - Q(\mathbf{o}_k^u, \mathbf{a}_k^u), \quad (11)$$

where γ is a discount factor; \hat{A}_k^u is an advantage function. Then, the critic network provides \hat{A}_k^u to the actor network to

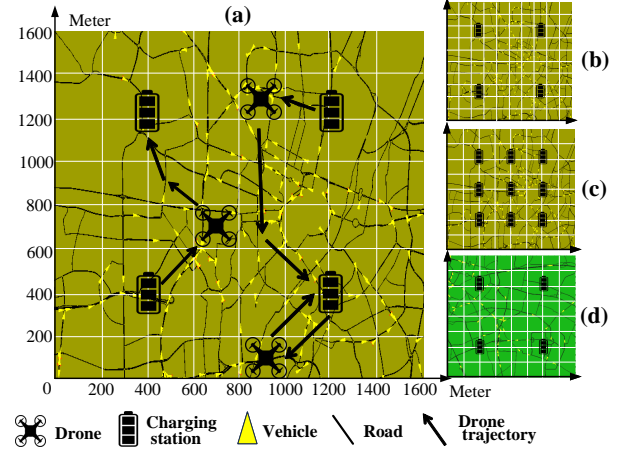


Fig. 5. The central business district of Munich, Germany: (a) Basic scenario with 64 cells, 4 charging stations and high density of vehicles; (b) Increase the number of cells to 100; (c) Increase the number of charging stations to 9; (d) Change to a new map with low density of vehicles.

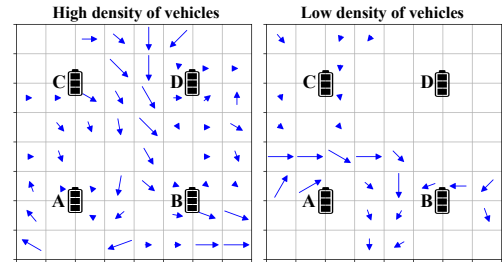


Fig. 6. The distribution of both charging stations and traffic vehicles in the maps with high and low density of vehicles. There are 4 charging stations uniformly distributed in the map with $64 = 8 \times 8$ cells lined up over the map. The blue arrows symbolize the flow of vehicular traffic, with their length proportional to the volume of vehicles over 8 periods.

increase the probability of actions that have a positive impact and decrease the ones that have negative impact. The actions are taken by drones as $\mathbf{a}_t^u = \pi(\mathbf{o}_t^u)$. The parameter θ^π of the actor network is updated by maximizing the clip objective $L_{CLIP}(\theta^\pi)$, as follows [37]:

$$L_{CLIP}(\theta^\pi) = \frac{1}{H \cdot U} \sum_{k=1}^H \sum_{u=1}^U \min(\text{ratio}(\theta^\pi, u) \hat{A}_k^u, \text{clip}(\text{ratio}(\theta^\pi, u), 1 - \epsilon, 1 + \epsilon) \hat{A}_k^u), \quad (12)$$

where ϵ is a hyperparameter; $\text{clip}(\cdot)$ defines the surrogate objective by limiting the range of $\text{ratio}(\theta^\pi, u) = \frac{\pi(\mathbf{a}_k^u | \mathbf{o}_k^u)}{\pi_{old}(\mathbf{a}_k^u | \mathbf{o}_k^u)}$ using clipping, thereby eliminating incentives to exceed the interval $[1 - \epsilon, 1 + \epsilon]$; π_{old} denotes the older policy of the actor network in the previous iteration.

VI. PERFORMANCE EVALUATION

In this section, an overview of the experimental settings is presented. The sensor dataset, specification of drones, optimization algorithm employed, and the used neural network are introduced. Then, the baselines and performance evaluation metrics are discussed. Finally, the results are assessed across various scenarios.

A. Experimental Settings

Scenario model. In order to evaluate the *DO-RL*, we model a real-world transportation scenario, where a swarm of drones perform the sensing tasks of traffic monitoring. The number of vehicles serves as the required sensing value in the model. The scenario involves a real-world map of Munich city, imported to the simulations of urban mobility (SUMO)² to accurately generate realistic flows of vehicles. Fig. 5 illustrates a selected map of 1600×1600 meters in the city with the simulation time of 50 hours, which is 100 periods. It has a high density of vehicles, approximately 2,000 vehicles passing by per hour. The area split into a finite number of cells, each is defined as a rectangular square with the size of 200×200 meters that can be captured by the cameras of drones. Fig. 6 shows the distribution of both charging stations and traffic vehicles in the map. The charging stations are uniformly distributed in the map. We employ cross-validation: 80% simulation time of the datasets for training and 20% for testing. There are two scenarios for the experimental evaluation in this paper: (i) *Basic scenario*. It has 64 cells, 4 charging stations and 8 time periods (set as 30min for each period). It has high density of vehicles, around 2,000 vehicles passing by per time period. 16 drones sense the area (camera recording) in parallel. (ii) *Complex scenario*. It varies the parameter settings such as the density of drones and vehicles, as well as the number of time periods, cells and charging stations. Noted that the simulated traffic flow can be displayed in a big screen in a testbed experimentation using hardware to emulate the complex outdoor sensing environments, which has been proved by our previous work in [15], [34].

Drones. We use DJI Phantom 4 Pro model³. Each drone has a body weight of 1.07 kg and four propellers, each with a diameter of 0.35 m. The ground speed of the drones is set at 6.94 m/s, and the drag force is determined to be 4.1134 N [36]. As a consequence, the power consumption remains consistent across all drones. Additionally, drones are equipped with a 6000 mAh LiPo 2S battery (0.31 kg). The maximum flying time for drones is approximately 30 min, which is set as one flying period. A flying period has $S = 30$ timeslots, each of one minute. Moreover, to ensure that the camera covers the entire area of a cell (see Fig. 5), the minimum hovering height of drones is determined at which the field of view of the camera and the cell overlap. The hovering height h is calculated based on the distance between any two cells (approximately 200 meters), the camera resolution, focal length derived from camera calibration, and ground sampling distance [38]. Therefore, each drone equipped with a 4K camera senses from a minimum height of 82.4 meters.

Planning and distributed optimization. We leverage the decentralized multi-agent collective learning method of *EPOS*⁴, the *Economic Planning and Optimized Selections* [7]. We generate $L = 64$ plans for each agent. All generated plans are made openly available to encourage further research on

coordinated spatio-temporal sensing of drones [12], [15], [24]. Each agent in *EPOS* is mapped to a drone. During the coordinated plan selection via *EPOS*, agents self-organize into a balanced binary tree as a way of structuring efficient learning interactions [39]. The shared goal of the agents is to minimize the RMSE between the total sensing values collected and the target via Eq.(7). In the one execution of *EPOS*, the agents perform 40 bottom-up and top-down learning iterations during which RMSE converges to a minimum optimized value.

Neural network and learning algorithm. In our problem, the weight parameters α_1 , α_2 and α_3 are all set to a value of 1. A total of $H = 64$ groups of transitions are sampled as minibatches in a replay buffer, with a discount factor of $\gamma = 0.95$ and a clip interval hyperparameter of 0.2 for policy updating. We try the recurrent neural network (RNN), and use $W = 64$ neurons in the three hidden layers of the RNN in both critic and actor networks. The activation function used for the networks is tanh. The models are trained over $\mathcal{E} = 5000$ episodes, each consisting of multiple epochs (equal to the number of time periods).

Complexity. Given the number of nodes per layer W , number of episodes \mathcal{E} , size of state space \mathcal{X} , and number of actions A , the computational complexity of DNN is approximately $O(C_{dnn}) := O((\mathcal{X} + A)W + 3W^2)$ [25]. The comparison of both computational and communication cost is shown in Table II, where I denotes the number of iterations in *EPOS*. The results illustrate that *DO-RL* significantly lowers the computation cost by reducing the number of actions required during training on a temporal scale, compared to the state-of-the-art *MAPPO*. *DO-RL* also has low communication cost due to the tree communication structure.

TABLE II
COMPARISON OF COMPUTATIONAL AND COMMUNICATION COSTS.

Attributes	Approaches:	<i>EPOS</i> [7]	<i>MAPPO</i> [16]	<i>DO-RL</i>
Computational Cost		$O(LI \log U)$	$O(ETSC_{dnn})$	$O(ET(C_{dnn} + LI \log U))$
Communication Cost		$O(I \log U)$	$O(U^2)$	$O(I \log U)$

B. Baselines and Metrics

We compare *DO-RL* with the following baseline methods:

Greedy. It aims to assign each drone to a single cell, enabling it to accomplish the necessary sensing tasks within a time period [20]. This algorithm minimizes the number of visited cells and travel distance, resulting in reduced energy consumption for drones. To promote decentralization, we implement the algorithm with a local view for each drone, i.e., they have no coordination or awareness of cell occupancy by other drones. By adopting this approach, we ensure an energy-efficient and independent operation of each drone.

EPOS. It is designed to select the optimal plan for drones based on the generated plans [7]. It incorporates the plan generation and the periodic state update, but does not support any long-term strategic navigation. Agents randomly choose any charging station to land on at every period.

MAPPO. It is one state-of-the-art DRL algorithm using PPO [16], [37], but does not include distributed optimization

²<https://www.eclipse.org/sumo/>

³<https://www.dji.com/uk/phantom-4-pro/info>

⁴*EPOS* is open-source and available at: <https://github.com/epoumaras/EPOS>.

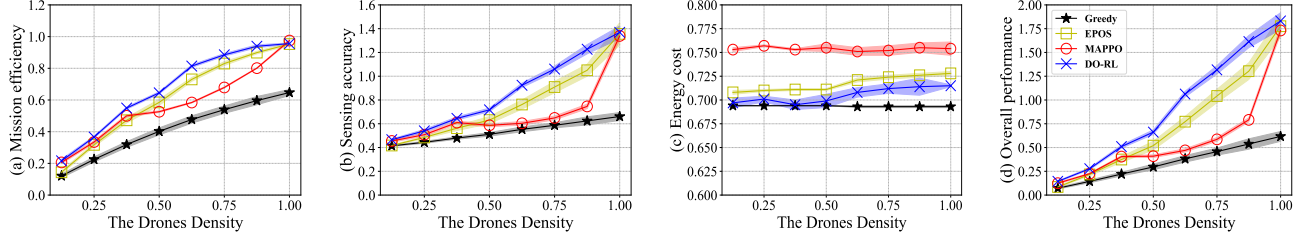


Fig. 7. **High density of drones increases both mission efficiency and sensing accuracy of all methods, especially for short-term optimization methods (*DO-RL* and *EPOS*).** *DO-RL* also shows its superior performance across different drones densities. Changing the drones density by increasing the number of drones from 8 to 64 and fixing 8 periods, 64 cells, 4 charging stations and high density of vehicles.

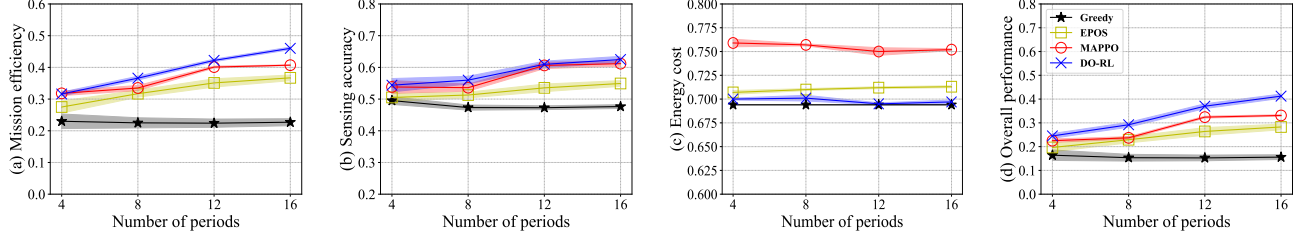


Fig. 8. **High number of periods increases both mission efficiency and sensing accuracy of all methods, especially for long-term learning methods (*DO-RL* and *MAPPO*).** *DO-RL* also shows its superior performance across different number of periods. Changing the the number of periods from 4 to 16 and fixing 16 drones, 64 cells, 4 charging stations and high density of vehicles.

compared to *DO-RL*. Moreover, agents in *MAPPO* learn the flying directions timeslot by timeslot, rather than period by period as in *DO-RL*. At each timeslot, a drone takes actions to horizontally move to an adjacent cell in eight directions or hover (similar to the actions in *DO-RL*), and returns to the nearest charging station at the end of every S timeslots (one period). For fair comparison, this method employs the same reward function and structured tree communication model to share the aggregated observation.

The evaluation of all algorithms includes three key metrics: 1) *Mission efficiency*, 2) *Sensing accuracy* and 3) *Energy cost*. These metrics are determined using Eq.(3), (4) and (5) respectively. We use the number of vehicles detected/observed by drones to represent the sensing values defined in this paper. Furthermore, to obtain a comprehensive assessment that considers all three metrics, we conduct an overall performance evaluation using Eq.(6).

C. Results and Analysis

There are six dimensions for the complex scenario we study here: (i) the density of drones, (ii) the number of periods, (iii) the number of cells, (iv) the number of charging stations, (v) the density of vehicles, (vi) the number of drones and cells while fixing the density of drones, (vii) the remaining battery level, and (viii) the charging load. Results are shown in Fig. 7-12, where the shadow area around the lines represents the standard deviation error of the results.

Density of drones. It denotes the ratio of the number of drones over the number of cells, representing the coverage of a single drone over the map. In this case, we fix the number of cells as 64, and increase the number of drones from 8 to 64, that is, the drones density increases from 0.125 to 1.0. Fig. 7 illustrates

the performance of *DO-RL* and baseline methods when using different drones density to perform traffic monitoring. As drones density increases, both mission efficiency and sensing accuracy of *DO-RL* increase linearly. These are approximately 23.0% and 15.8% higher than *EPOS* respectively, as shown in Fig. 7(a) and Fig. 7(b) ⁵. This is because *DO-RL* controls the traveling direction of drones based on the predicted sensor data, so that drones cover the area with the maximum sensing value. *MAPPO* has high efficiency and accuracy with a low density of drones (maximum p-value less than 0.001 using Mann-Whitney U test), but its performance degrades when the drones density is higher than 0.375 due to the high computational complexity. In contrast, the plan selection in *DO-RL* reduces the action space and mitigates the learning difficulty, resulting in high performance with a high number of drones. In Fig. 7(c), the energy cost of *DO-RL* is on average 1.7% lower than *EPOS* and 7.9% lower than *MAPPO*. *Greedy* has the minimum energy cost among all methods, only 7.89% lower than *DO-RL*, but has the lowest performance in efficiency and accuracy. *DO-RL* sacrifices a little energy for sensing, but still gets lower cost than other methods.

Number of periods. As shown in Fig. 8, *DO-RL* achieves superior performance compared to other methods, increasing linearly as the number of periods increase (increased by 51.3% in quadruple time). Although it has statistically similar mission efficiency to *MAPPO* when the number of periods is 4, this metric increases dramatically because drones update and obtain more accurate predicted sensor data with higher number of periods. The timeslot-by-timeslot learning

⁵*DO-RL*, *EPOS* and *MAPPO* have similar overall performance when drones density is 1.0, with maximum p-value of 0.04, because there are ample drone resources available to effectively coordinate the coverage of the map.

	Mission Efficiency				Sensing Mismatch				Energy Cost				Overall Performance																			
	Greedy	EPOS	MAPPO	DO-RL	Greedy	EPOS	MAPPO	DO-RL	Greedy	EPOS	MAPPO	DO-RL	Greedy	EPOS	MAPPO	DO-RL																
cells=64 stations=4	0.23	0.23	0.32	0.32	0.34	0.51	0.34	0.53	0.47	0.48	0.51	0.51	0.54	0.82	0.61	0.93	0.69	0.69	0.71	0.71	0.75	0.77	0.71	0.71	0.16	0.17	0.23	0.23	0.24	0.55	0.29	0.69
cells=100 stations=4	0.15	0.15	0.17	0.20	0.19	0.36	0.27	0.40	0.53	0.53	0.53	0.54	0.56	0.86	0.60	0.88	0.69	0.69	0.71	0.71	0.75	0.75	0.70	0.70	0.12	0.12	0.13	0.15	0.14	0.42	0.23	0.49
cells=64 stations=9	0.23	0.23	0.29	0.29	0.40	0.50	0.31	0.57	0.47	0.47	0.49	0.49	0.59	0.84	0.52	0.89	0.69	0.69	0.71	0.71	0.74	0.75	0.70	0.70	0.16	0.16	0.20	0.20	0.32	0.56	0.23	0.72
cells=100 stations=9	0.15	0.15	0.20	0.21	0.19	0.31	0.28	0.47	0.53	0.52	0.54	0.55	0.56	0.83	0.60	0.98	0.69	0.69	0.70	0.71	0.75	0.75	0.70	0.70	0.12	0.12	0.15	0.17	0.14	0.34	0.24	0.66
	High	Low	High	Low	High	Low	High	Low	High	Low	High	Low	High	Low	High	Low	High	Low	High	Low	High	Low	High	Low	High	Low	High	Low	High	Low	High	Low

Fig. 9. Both low number of cells and high number of charging stations increase the overall performance of all methods. Long-term learning methods outperform short-term optimization methods in observing traffic flow when vehicles are sparsely distributed across the map. Performance comparison under varying parameters: the number of cells (64 and 100), the number of charging stations (4 and 9), and the density of vehicles (high and low). The red palette on the right represents the values of energy cost, while the blue one denotes the values of mission efficiency, sensing mismatch and overall performance.

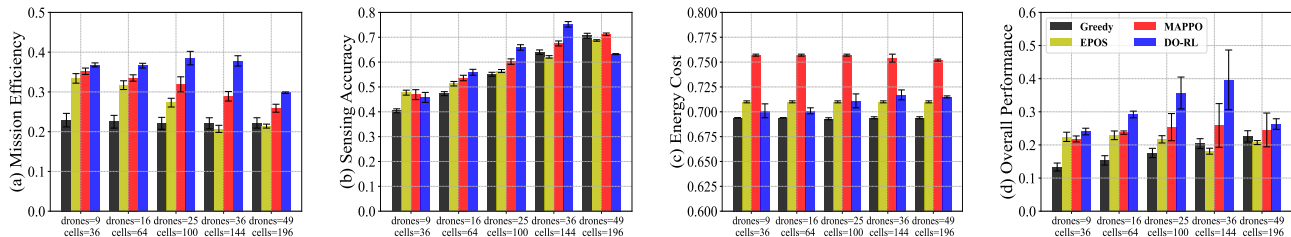


Fig. 10. High number of drones/cells with fixed drones density increases the sensing accuracy of all methods, peaking at 36 drones and 144 cells. Changing the number of drones and cells but fixing the drones density at 0.25 with 8 periods, 4 charging stations and high density of vehicles.

in *MAPPO* perplexes the actions learned by drones compared to *DO-RL*, since drones only take actions once per period (30min) in *DO-RL* but take actions per minute in *MAPPO*. This also results in higher flying energy consumed by drones, and thus the energy cost of *MAPPO* is around 8.1% higher than *DO-RL*.

Fig. 9 illustrates the performance comparison between *DO-RL* and baseline methods, varying the number of cells, charging stations and the density of vehicles, while keeping the number of drones fixed at 16 and periods at 8.

Number of cells. If the number of cells increases from 64 to 100, the density of drones decreases. In Fig. 9, *DO-RL* shows a lower decrease in mission efficiency (decreased by 27.04%) than *MAPPO* (decreased by 44.50%) and *EPOS* (decreased by 45.11%) as the number of cells increases. Furthermore, *DO-RL* keeps relatively constant both sensing accuracy and energy cost as the number of cells varies.

Number of charging stations. If the number of charging stations increases from 4 to 9, the distance between the sensing areas and stations is reduced, cutting down the energy cost of recharging. As a result, the overall performance of both *DO-RL* and *EPOS* increase by 19.52% and 14.35% respectively.

Density of vehicles. If we select a new map area that has low density of vehicles, the distribution of sensor data changes (with different road distribution), as shown in Fig. 6. In Fig. 9, both *DO-RL* and *MAPPO* have higher mission efficiency and sensing accuracy than the other two methods, with an average of 90.65% higher efficiency and 76.85% higher accuracy. This is because the learning methods observe the environment and control drones to collect data in cells and timeslots with the highest number of vehicles. *DO-RL* performs better than other

methods under low vehicle density even though the number of cells and charging stations increase.

Number of drones/cells with fixed drones density. If we fix the density of drones but increase the number of drones, the number of cells increases proportionally. For example, we use the density of drones in the basic scenario of 0.25, and increase the number of drones from 9 to 49 and the number of cells from 36 to 196. As shown in Fig. 10, when the number of drones/cells increases, the sensing accuracy of all methods increases. However, the mission efficiency of both *EPOS* and *MAPPO* decreases (by 35.93% and 26.42% respectively). This is due to *EPOS* facing challenges in efficiently scheduling drones for a large number of cells, while *MAPPO* experiences increased computational complexity. In contrast, *DO-RL* overcomes these challenges and demonstrates a 4.62% increase in mission efficiency. When increasing to 49 drones and 196 cells, however, the sensing accuracy of *DO-RL* degrades, decreased by 15.96%, due to the high complexity of scheduling and computation. In overall, *DO-RL* has statistically higher overall performance than other methods, with an average improvement of 46.98% (maximum p-value less than 0.001).

Remaining battery level. It denotes a percentage of battery level once drones have completed their sensing tasks. The value is calculated as an average among all drones within each time period. As shown in the Fig. 11(a) and 11(b), *DO-RL* keeps drones at a high remaining battery level on high and low density of vehicles, with approximately 30.25% and only 1.05% lower than *Greedy*. This level follows the drones' safety regulations which suggest finishing the missions when battery life is around 25% – 30%. However, *MAPPO* does not

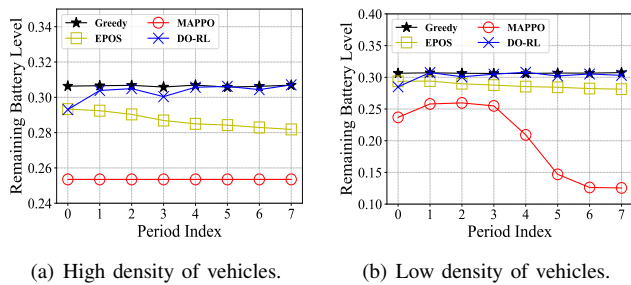
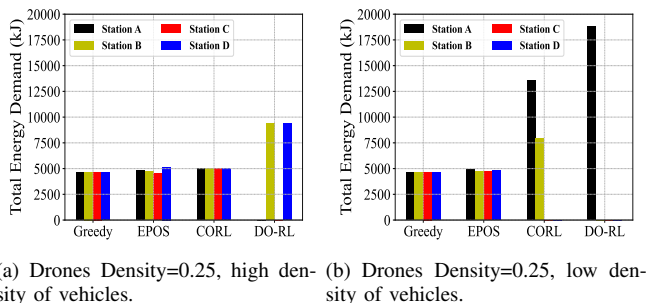
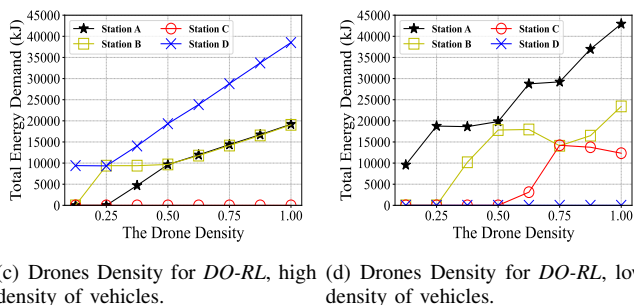


Fig. 11. *DO-RL* keeps drones at a safe remaining battery level before recharging. Performance comparison of the remaining battery level of four methods on both high and low density of vehicles.



(a) Drones Density=0.25, high density of vehicles. (b) Drones Density=0.25, low density of vehicles.



(c) Drones Density for *DO-RL*, high density of vehicles. (d) Drones Density for *DO-RL*, low density of vehicles.

Fig. 12. *DO-RL* relies on a lower number of charging places compared to other methods. Performance comparisons of the total energy demand of four methods with 0.25 density of drones, see (a) and (b), and the *DO-RL* with different density of drones, see (c) and (d). Both comparisons are categorized by the high and low density of vehicles, see Fig. 6.

meet the regulations under low density of vehicles, and the minimum battery level can reach 12.55%.

Charging load. It is the total energy demand of drones on each charging station over all time periods. This aims to study the placement of charging stations. As shown in the Fig. 12(a) and 12(b), the total energy demand on charging stations of *DO-RL* over all periods is more imbalanced compared to other methods. This is because with *DO-RL* drones learn to travel to the areas with the high required sensing data values. Since drones set the nearest charging stations as destinations, they rely on a lower number of charging places. For example, as shown in Fig. 12(c) and 12(d), when the density of drones is 0.125 under high density of vehicles, drones only depart from and return to the charging station *D* since the vehicle distribution around *D* is more dense than other charging stations. As the density of drones becomes 1, drones gradually rely on the charging station *B* and *D*. Similarly, drones only

need to fly over the vehicle-dense areas around the charging station *A* and *B* under low density of vehicles. These results provide insights to policy makers for providing higher amount of energy on vehicle-dense areas to support drones' charging.

In summary, **several scientific insights** on experimental results are listed as follows: (i) Under scarce drone resources, it is more efficient and accurate to employ long-term learning methods for optimizing sensing. In contrast, under abundant drone resources, short-term optimization methods alone suffice. (ii) Long-term learning methods optimize drone resources usage for traffic management by directing drones towards regions with high vehicle density and advising on infrastructure planning for charging. (iii) Short-term optimization aids long-term learning by simplifying agent coordination, enhancing sensing quality, and preventing energy waste. This approach ensures that drones operate efficiently while maintaining battery levels above safety thresholds, leading to more reliable and effective missions.

VII. CONCLUSION AND FUTURE WORK

This paper studies a large-scale spatio-temporal task assignment problem by a swarm of autonomous drones. We propose a new synergetic optimization approach named *DO-RL*, by integrating both evolutionary distributed optimization and DRL, to solve the problem by optimizing the flight paths, data collection and recharging assignment of drone swarms. In each time period, drones determine their overall flying directions to destinations with charging stations via DRL, and autonomously evolve their navigation and sensing plans using collective learning. Extensive experimentation using realistic urban mobility reveals the effectiveness of *DO-RL* and provides valuable insights for the broader community: The combination of short-term and long-term strategies proves highly effective in overcoming their standalone limitations in drone-based traffic monitoring. Short-term methods compensate the challenges of training complexity, energy consumption and recharging, while long-term approaches account for maximizing accumulated rewards, enhancing the overall sensing performance. This collaborative approach allows the system to dynamically adapt to changing environments, efficiently managing varying drone resources and enabling extended operations.

However, the designed framework can be further improved towards several research avenues: 1) Use of simulated and real-world datasets in other applications, such as disaster response. 2) Consideration of more realistic factors such as obstacles and charging capability. 3) Research of the real-time drone testbed to validate the applicability of the proposed method.

ACKNOWLEDGEMENTS

This research is supported by a UKRI Future Leaders Fellowship (MR/W009560/1): *Digitally Assisted Collective Governance of Smart City Commons-ARTIO*, and the European Union, under the Grant Agreement GA101081953 for the project H2OforAll—*Innovative Integrated Tools and Technologies to Protect and Treat Drinking Water from Disinfection Byproducts (DBPs)*. Views and opinions expressed are, however, those of the author(s) only and do not necessarily reflect those of the European Union.

Neither the European Union nor the granting authority can be held responsible for them. Funding for the work carried out by UK beneficiaries has been provided by UKRI under the UK government's Horizon Europe funding guarantee [grant number 10043071]. Thanks to Manos Chaniotakis and Zeinab Nezami for the support on the transportation datasets.

REFERENCES

- [1] Lingyun Zhou, Daniel F Silva, and Alice E Smith. Locating drone stations for a truck-drone delivery system in continuous space. *IEEE Transactions on Evolutionary Computation*, 2023.
- [2] Emmanouil Barmponakis and Nikolas Geroliminis. On the new era of urban traffic monitoring with massive drone data: The pneuma large-scale field experiment. *Transportation research part C: emerging technologies*, 111:50–71, 2020.
- [3] Min Deng, Baoju Liu, Sumin Li, Ronghua Du, Guohua Wu, Haifeng Li, and Ling Wang. A two-phase coordinated planning approach for heterogeneous earth-observation resources to monitor area targets. *IEEE Transactions on Systems, Man, and Cybernetics: Systems*, 51(10):6388–6403, 2020.
- [4] Sabitri Poudel and Sangman Moh. Task assignment algorithms for unmanned aerial vehicle networks: A comprehensive survey. *Vehicular Communications*, page 100469, 2022.
- [5] Yongkun Zhou, Bin Rao, and Wei Wang. Uav swarm intelligence: Recent advances and future trends. *Ieee Access*, 8:183856–183878, 2020.
- [6] Jingjing Cui, Yuanwei Liu, and Arumugam Nallanathan. Multi-agent reinforcement learning-based resource allocation for UAV networks. *IEEE Transactions on Wireless Communications*, 19(2):729–743, 2019.
- [7] Evangelos Pournaras, Peter Pilgerstorfer, and Thomas Asikis. Decentralized collective learning for self-managed sharing economies. *ACM Transactions on Autonomous and Adaptive Systems*, 13(2):1–33, 2018.
- [8] Evangelos Pournaras. Collective learning: A 10-year odyssey to human-centered distributed intelligence. In *2020 IEEE International Conference on Autonomic Computing and Self-Organizing Systems (ACSOS)*, pages 205–214. IEEE, 2020.
- [9] Srijoni Majumdar, Chuhao Qin, and Evangelos Pournaras. Discrete-choice multi-agent optimization: Decentralized hard constraint satisfaction for smart cities. *International Conference on Autonomous Agents and Multiagent Systems*. Springer, 2023.
- [10] Evangelos Pournaras, Srivatsan Yadhunathan, and Ada Diaconescu. Holarchic structures for decentralized deep learning: a performance analysis. *Cluster Computing*, 23(1):219–240, 2020.
- [11] Jovan Nikolic and Evangelos Pournaras. Structural self-adaptation for decentralized pervasive intelligence. In *22nd Euromicro Conference on Digital System Design (DSD)*, pages 562–571. IEEE, 2019.
- [12] Chuhao Qin and Evangelos Pournaras. EPOS-based Plans for Iterative Sensing and Charging. 11 2023. doi = "https://doi.org/10.6084/m9.figshare.24476533.v2".
- [13] Mehdi Alighanbari and Jonathan How. Robust decentralized task assignment for cooperative UAVs. In *AIAA Guidance, Navigation, and Control Conference and Exhibit*, page 6454, 2006.
- [14] Jie Chen, Xianguo Qing, Fang Ye, Kai Xiao, Kai You, and Qian Sun. Consensus-based bundle algorithm with local replanning for heterogeneous multi-UAV system in the time-sensitive and dynamic environment. *The Journal of Supercomputing*, 78(2):1712–1740, 2022.
- [15] Chuhao Qin, Fethi Candan, Lyudmila Mihaylova, and Evangelos Pournaras. 3, 2, 1, drones go! a testbed to take off uav swarm intelligence for distributed sensing. In *UK Workshop on Computational Intelligence*, pages 576–587. Springer, 2022.
- [16] Lige Ding, Dong Zhao, Mingzhe Cao, and Huadong Ma. When crowd-sourcing meets unmanned vehicles: Toward cost-effective collaborative urban sensing via deep reinforcement learning. *IEEE Internet of Things Journal*, 8(15):12150–12162, 2021.
- [17] Dong Zhao, Mingzhe Cao, Lige Ding, Qiaoyue Han, Yunhao Xing, and Huadong Ma. Dronesense: Leveraging drones for sustainable urban-scale sensing of open parking spaces. In *IEEE INFOCOM - Conference on Computer Communications*, pages 1769–1778. IEEE, 2022.
- [18] Pengyi Li, Jianye Hao, Hongyao Tang, Yan Zheng, and Xian Fu. Race: improve multi-agent reinforcement learning with representation asymmetry and collaborative evolution. In *International Conference on Machine Learning*, pages 19490–19503. PMLR, 2023.
- [19] Moataz Samir, Chadi Assi, Sanaa Sharafeddine, Dariush Ebrahimi, and Ali Ghraryeb. Age of information aware trajectory planning of UAVs in intelligent transportation systems: A deep learning approach. *IEEE Transactions on Vehicular Technology*, 69(11):12382–12395, 2020.
- [20] Novella Bartolini, Andrea Coletta, and Gaia Maselli. On task assignment for early target inspection in squads of aerial drones. In *2019 IEEE 39th International Conference on Distributed Computing Systems (ICDCS)*, pages 2123–2133. IEEE, 2019.
- [21] Qiang Yang, Gong-Wei Song, Wei-Neng Chen, Ya-Hui Jia, Xu-Dong Gao, Zhen-Yu Lu, Sang-Woon Jeon, and Jun Zhang. Random contrastive interaction for particle swarm optimization in high-dimensional environment. *IEEE Transactions on Evolutionary Computation*, 2023.
- [22] Ahmed Awad, Amjad Hawash, and Baker Abdalhaq. A genetic algorithm (ga) and swarm-based binary decision diagram (bdd) reordering optimizer reinforced with recent operators. *IEEE Transactions on Evolutionary Computation*, 27(3):535–549, 2022.
- [23] Shayegan Omidshafiei, Ali-Akbar Agha-Mohammadi, Christopher Amato, Shih-Yuan Liu, Jonathan P How, and John Vian. Decentralized control of multi-robot partially observable markov decision processes using belief space macro-actions. *The International Journal of Robotics Research*, 36(2):231–258, 2017.
- [24] Chuhao Qin and Evangelos Pournaras. Coordination of drones at scale: Decentralized energy-aware swarm intelligence for spatio-temporal sensing. *Transportation Research Part C: Emerging Technologies*, 157:104387, 2023.
- [25] Babatunji Omoniwa, Boris Galkin, and Ivana Dusparic. Communication-enabled deep reinforcement learning to optimise energy-efficiency in UAV-assisted networks. *Vehicular Communications*, 43:100640, 2023.
- [26] Pengyi Li, Jianye Hao, Hongyao Tang, Xian Fu, Yan Zhen, and Ke Tang. Bridging evolutionary algorithms and reinforcement learning: A comprehensive survey on hybrid algorithms. *IEEE Transactions on Evolutionary Computation*, 2024.
- [27] Somdeb Majumdar, Shauharda Khadka, Santiago Miret, Stephen McAleer, and Kagan Tumer. Evolutionary reinforcement learning for sample-efficient multiagent coordination. In *International Conference on Machine Learning*, pages 6651–6660. PMLR, 2020.
- [28] Ayhan Alp Aydeniz, Robert Loftin, and Kagan Tumer. Novelty seeking multiagent evolutionary reinforcement learning. In *GECCO*, pages 402–410, 2023.
- [29] Bei Peng, Tabish Rashid, Christian Schroeder de Witt, Pierre-Alexandre Kamienny, Philip Torr, Wendelin Böhmer, and Shimon Whiteson. Facmac: Factored multi-agent centralised policy gradients. *Advances in Neural Information Processing Systems*, 34:12208–12221, 2021.
- [30] Mikayel Samvelyan, Tabish Rashid, Christian Schroeder de Witt, Gregory Farquhar, Nantas Nardelli, Tim GJ Rudner, Chia-Man Hung, Philip HS Torr, Jakob Foerster, and Shimon Whiteson. The starcraft multi-agent challenge. In *18th AAMAS*, pages 2186–2188, 2019.
- [31] Mouna Elloumi, Riadh Dhaou, Benoit Escrig, Hanen Idoudi, and Leila Azouz Saidane. Monitoring road traffic with a UAV-based system. In *2018 IEEE Wireless Communications and Networking Conference (WCNC)*, pages 1–6. IEEE, 2018.
- [32] David Castells-Graells, Christopher Salahub, and Evangelos Pournaras. On cycling risk and discomfort: urban safety mapping and bike route recommendations. *Computing*, 102:1259–1274, 2020.
- [33] Jun Tang, Songyang Lao, and Yu Wan. Systematic review of collision-avoidance approaches for unmanned aerial vehicles. *IEEE Systems Journal*, 16(3):4356–4367, 2021.
- [34] Chuhao Qin, Alexander Robins, Callum Lillywhite-Roake, Adam Pearce, Hritik Mehta, Scott James, Tsz Ho Wong, and Evangelos Pournaras. M-SET: Multi-drone swarm intelligence experimentation with collision avoidance realism. *1st IEEE LCN Special Track on Algorithmic Solutions for Drone- and Robot-based Networks (ASDRoNet)*, 2024.
- [35] Ana Batinovic, Jurica Goricanec, Lovro Markovic, and Stjepan Bogdan. Path planning with potential field-based obstacle avoidance in a 3d environment by an unmanned aerial vehicle. In *2022 International Conference on Unmanned Aircraft Systems (ICUAS)*, pages 394–401. IEEE, 2022.
- [36] Momena Monwar, Omid Semiari, and Walid Saad. Optimized path planning for inspection by unmanned aerial vehicles swarm with energy constraints. In *2018 IEEE Global Communications Conference (GLOBECOM)*, pages 1–6. IEEE, 2018.
- [37] Wenjie Yi, Rong Qu, Licheng Jiao, and Ben Niu. Automated design of metaheuristics using reinforcement learning within a novel general search framework. *IEEE Transactions on Evolutionary Computation*, 27(4):1072–1084, 2022.
- [38] Damian Wierzbicki. Multi-camera imaging system for UAV photogrammetry. *Sensors*, 18(8):2433, 2018.
- [39] Evangelos Pournaras. Multi-level reconfigurable self-organization in overlay services. 2013. Ph.D. Dissertation. TU Delft, Delft University of Technology.

TABLE III
NOTATIONS.

Notation	Explanation
u, U, \mathcal{U}	Index of a drone; total number of drones; set of drones
m, M, \mathcal{M}	Index of a charging station; total number of charging stations; set of charging stations
n, N, \mathcal{N}	Index of a grid cell; total number of grid cells; set of grid cells
s, S, \mathcal{S}	Index of a timeslot; total number of timeslots in a period; set of timeslots
t, T, \mathcal{T}	Index of a period; total number of periods; set of periods
a^u	The action or flying direction taken by u
$P^u, p_{n,s}^u$	The plan of u ; value of P^u at cell n and timeslot s
$P^{-u}, p_{n,s}^{-u}$	The observed plan of drones by u excluding P^u ; value of P^{-u} at cell n and timeslot s
$p_{n,s}$	The aggregated plans of all drones at cell n and timeslot s
$V_{n,s}$	Required sensing value at cell n and timeslot s
$v_{n,s}$	Collected sensing value at cell n and timeslot s
$\mathcal{R}, r_{n,s}$	Target; target value at cell n and timeslot s
l, L	Index of a plan in G^{a^u} ; total number of plans in G^{a^u}
$C^f(u), t^f$	Flying power consumption of u ; flying time
$C^h(u), t^h$	Hovering power consumption of u ; hovering time
$B(u)$	Battery capacity of u
$\alpha_1, \alpha_2, \alpha_3$	Weight parameters of mission efficiency, sensing accuracy and energy cost in the main objective function respectively
c^u, e^u	Current location of u ; current energy consumption of u
$K(a^u)$	Indexes of cells within the searching range along flying direction a^u
$J(a^u)$	Indexes of visited cells within $K(a^u)$
β	Behavior of an agent in planning optimization
o_t^u, r_t^u	Observation of u at period t ; reward of u at the period t
k, H	Index of a sampled transition; number of sampled transitions
γ, ϵ	Discount factor; clip interval hyperparameter
$Q(\cdot), \theta^Q$	Critic network; parameter of critic network
$\pi(\cdot), \theta^\pi$	Actor network; parameter of actor network
$\omega_{n,s}, \bar{v}$	Prediction coefficient to calculate $\hat{V}_{n,s}$; threshold to remove the regions with low sensing requirements
I, \mathcal{X}, A	Total number of iterations in <i>EPOS</i> ; size of state space; number of actions in DRL
\mathcal{E}, W	Number of episodes; number of neutrals per layer in DNN

APPENDIX A MATHEMATICAL NOTATIONS

Table III illustrates the list of mathematical notations used in this paper.

APPENDIX B PSEUDOCODE OF ALGORITHM

we present the pseudocode of the proposed *DO-RL* shown in Algorithm 1.

APPENDIX C EFFECT OF DIFFERENT PARAMETERS

The objective of this appendix is to analyze the impact of various parameters within the plan generation and distributed optimization of the proposed method. The insights derived from this appendix can be used to make informed empirical decisions regarding parameter selection for the evaluation scenarios. The calculations presented herein can be automated for any scenario during hyper-parameter optimization. Such optimization is not the focus of this paper.

We use the *DO-RL* and the basic scenario to test the mobility range and the agents' behavior.

Algorithm 1: DO-RL

```

1 Initialize critic network  $Q(\cdot)$ , actor network  $\pi(\cdot)$  with
  weights  $\theta^Q, \theta^\pi$ , and their two target networks  $Q'(\cdot),$ 
   $\pi'(\cdot)$  with parameters  $\theta^{Q'} := \theta^Q, \theta^{\pi'} := \theta^\pi$ ;
2 for  $episode := 1$  to  $max-episode-number$  do
3   Reset environment and obtain the initial state  $\mathbf{s}_1$ ;
4   for  $period t := 1$  to  $episode-length$  do
5     for  $drone u := 1, \dots, U$  do
6       Take action  $a_t^u = \pi(\mathbf{o}_t^u | \theta^\pi)$ ;
7       Select the set of plans  $G^{a^u}(t)$ ;
8       Pick a plan  $P^u(a^u, t)$  and share it with
        other drones via tree communication;
9       Observe the aggregated plan  $P^{-u}(a^u, t)$ 
        and pick an optimized plan through
        collective learning [7];
10      Compute reward  $\mathbf{r}_t^u =$ 
         $\alpha_1 \text{Eff}(a^u, t) + \alpha_2 \cdot \text{Acc}(a^u, t) - \alpha_3 E(a^u, t)$ ;
11      Store transition sample  $(\mathbf{o}_t^u, \mathbf{a}_t^u, \mathbf{r}_t^u, \mathbf{o}_{t+1}^u)$ 
        into buffer;
12      Sample a random minibatch of  $H$  samples
         $(\mathbf{o}_k^u, \mathbf{a}_k^u, \mathbf{r}_k^u, \mathbf{o}_{k+1}^u)$  from buffer;
13    end
14  end
15  Update  $\theta^Q$  by minimizing the loss function via
    Eq.(10);
16  Update  $\theta^\pi$  by maximizing the clip objective via
    Eq.(12);
17  Update the target networks:  $\theta^{Q'} \leftarrow \theta^Q, \theta^{\pi'} \leftarrow \theta^\pi$ ;
18 end

```

Mobility range. Fig. 13(a) illustrates the effect of different numbers of visited cells. The higher the number of cells a drone visits, the higher the flying energy is, and the higher the energy cost is. The high number of visited cells perplexes the spatio-temporal navigation and sensing of a drone, leading to over-sensing. Specifically, multiple drones visit the same cell simultaneously and waste energy on collecting the same data. In contrast, if drones visit only one cell, they are free from over-sensing, but have a high probability to miss the area with a high required sensing data due to its low mobility range. As a result, we empirically select $J(a^u) = 2$ for each drone to optimize the overall performance.

Agents' behavior. Fig. 13(b) illustrates the effect of agents' behavior by varying the parameter of β [7]. As β increases from 0 to 1, agents reduce the energy cost of their selected plans, while decreasing both efficiency and accuracy. This is because, according to Eq. 7, drones with higher β choose a plan with lower energy cost, which degrades the matching between the total sensing and the target. Since the overall performance for $\beta \in [0.1, 0.8]$ is statistically similar, using the Mann-Whitney U test with average p-value of 0.0003, drones are allowed to choose their behaviors within this range.

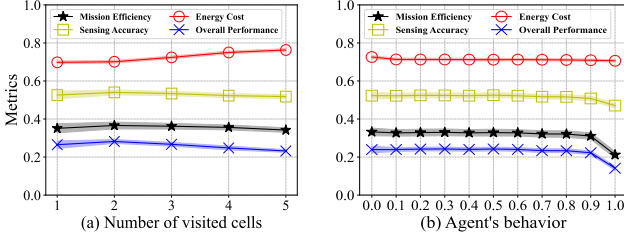


Fig. 13. *DO-RL* has its peak overall performance when $J_u = 2$, $\beta \in [0.1, 0.8]$. Change the parameters of *DO-RL* in mobility range and agents' behavior.

APPENDIX D POWER CONSUMPTION MODEL

Drones spend energy to surpass gravity force and counter drag forces due to wind and forward motions. A drone controls the speed of each rotor to achieve the thrust T and pitch θ necessary to stay aloft and travel forward at the desired velocity while balancing the weight and drag forces. For a drone with mass m_b and its battery with mass m_c , we define the total required thrust as follows:

$$\mathcal{T} = (m_b + m_c) \cdot g + F_d, \quad (13)$$

where g is the gravitational constant, and F_d is the drag force that depends on air speed and air density. For steady flying, the drag force can be calculated by the pitch angle θ as:

$$F_d = (m_b + m_c) \cdot g \cdot \tan(\theta). \quad (14)$$

Based on the model in [36], the power consumption with forward velocity and forward pitch is given by:

$$C^f = (v \cdot \sin\theta + v_i) \cdot \frac{\mathcal{T}}{\epsilon}, \quad (15)$$

where v is the average ground speed; ϵ is the overall power efficiency of the drone; v_i is the induced velocity required for given T and can be found by solving the nonlinear equation:

$$v_i = \frac{2 \cdot \mathcal{T}}{\pi \cdot d^2 \cdot r \cdot \rho \cdot \sqrt{(v \cdot \cos\theta)^2 + (v \cdot \sin\theta + v_i)^2}}, \quad (16)$$

where d and r are the diameter and number of drone rotors; ρ is the density of air.

Moreover, the power consumption for hovering of a drone is calculated by:

$$C^h = \frac{\mathcal{T}^{3/2}}{\epsilon \cdot \sqrt{\frac{1}{2} \pi \cdot d^2 \cdot n \cdot \rho}}. \quad (17)$$